Volume 2 | Number 29 | 7 August 2014 | Pages 4585–4756

Journal of Materials Chemistry B

Materials for biology and medicine

www.rsc.org/MaterialsB

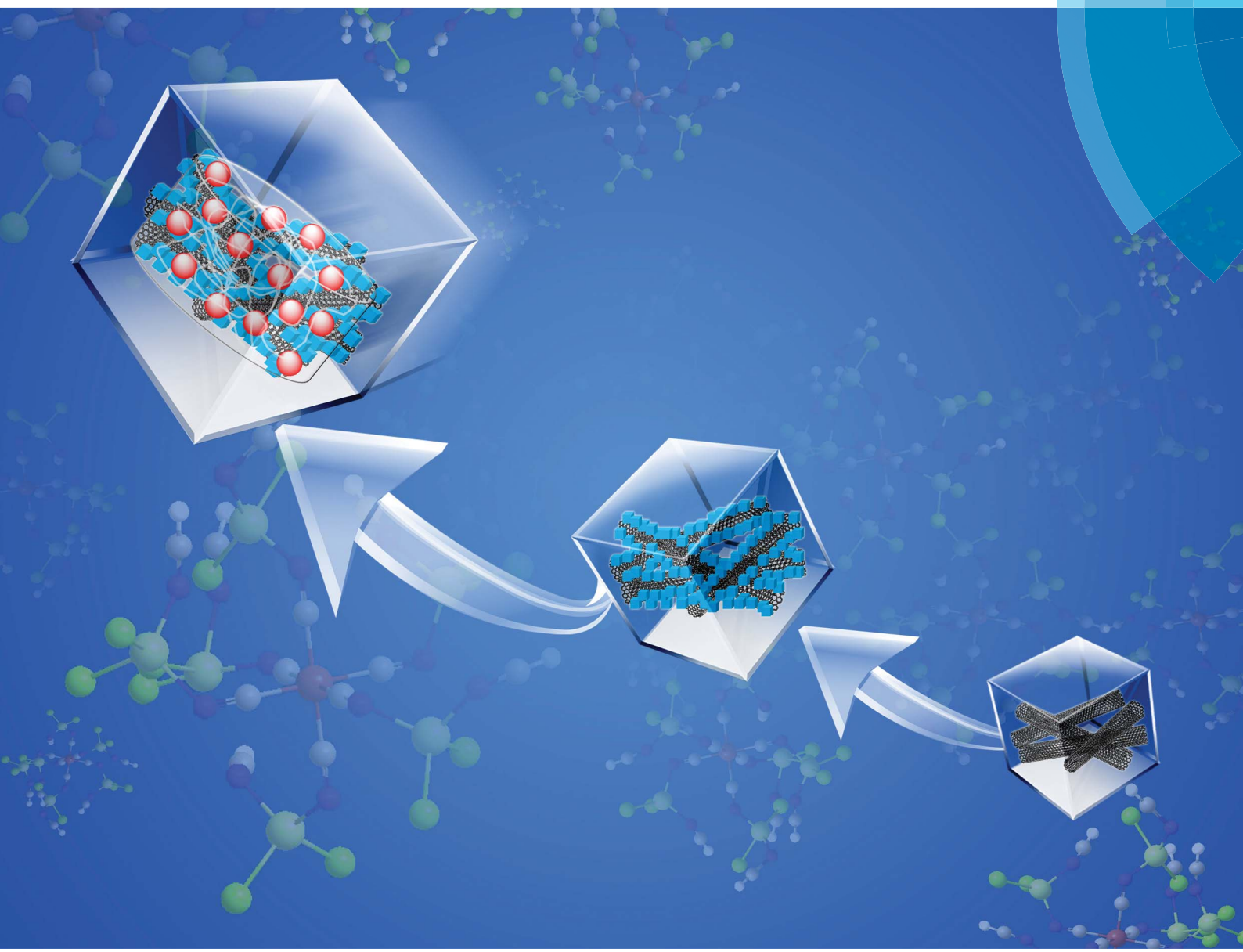

ISSN 2050-750X

ROYAL SOCIETY OF CHEMISTRY

PAPER

Dongmei Sun *et al.*

Sn–Fe cyanogels noncovalently grafted to carbon nanotubes in a versatile biointerface design: an efficient matrix and a facile platform for glucose oxidase immobilization

Journal of Materials Chemistry B

PAPER

View Article Online
View Journal | View Issue

Cite this: J. Mater. Chem. B, 2014, 2, 4615

Sn–Fe cyanogels noncovalently grafted to carbon nanotubes in a versatile biointerface design: an efficient matrix and a facile platform for glucose oxidase immobilization†

Hailing Liu,‡ Baoping Chen,‡ Dongmei Sun,* Yiming Zhou, Yawen Tang, Yu Chen and Tianhong Lu

Received 13th March 2014
Accepted 23rd April 2014

DOI: 10.1039/c4tb00406j

www.rsc.org/MaterialsB

Enzyme immobilization is a powerful strategy adapted to effectively maximize the bioactivity, specificity and stability of an isolated enzyme. In this study, we demonstrate a novel and scalable procedure for facile enzyme immobilization, in which three-dimensional porous Sn–Fe hydrogels were applied to incorporate the enzyme to construct a sensing interface for an amperometric biosensor. The process was initiated from the electrodeposition of Prussian Blue (PB) on multi-walled carbon nanotube (MWCNT)-modified gold electrodes, sequentially capped with tin tetrachloride ($SnCl_4$) solution followed by the addition of a freshly-made homogeneous mixture of enzyme and potassium ferrocyanide solution, leading to instant formation of hydrated three-dimensional (3D) porous Sn–Fe cyanogel networks, deeply set outside the produced rough layer of the MWCNT–PB complexes, providing a desirable microenvironment for the entrapped enzyme. The structural morphology and electrochemical properties of the as-prepared Sn–Fe cyanogels noncovalently grafted to MWCNTs with functionalities of electrodeposited PB were well characterized by scanning electron microscopy (SEM), ultraviolet visible spectroscopy (UV-vis) and cyclic voltammetry. The results indicate that the modified electrode with a multilayer configuration was well-organized, as proposed, and exhibited good electrical conductivity and stable catalytic activity to H_2O_2 electro-reduction due to the functional layer of PB. When glucose oxidase (GOx) was selected as a model enzyme, the resulting glucose biosensor exhibited a relatively low detection limit of 0.1 μM (S/N 3) with a good sensitivity of 1.68 μA mM^{-1} cm^{-2} and improved stability. The results suggest that the Sn–Fe cyanogels, with sufficient interfacial adhesion, hold promise as an attractive support material.

Introduction

Enzymes, which are eco-friendly and sustainable from renewable sources of living organisms, known as the most efficient versatile biocatalysts with incredible selectivity towards individual substrates, have attracted much attention and play increasingly vital roles from fundamental research to practical applications[1–5] such as biotransformation, biosensing, green energy supplies and organic syntheses, *etc*. It is expected that, with the fast-growing techniques of recombinant DNA, most enzymes, in principle, could be produced on a large-scale with an economically competitive price in the near future. However, enzymes *in vitro*,[6] especially operated in the liquid phase, are fragile, and the native conformation is prone to be compromised or further degraded through disruption of its surrounding noncovalent interactions under undesired environmental conditions, therefore irreversibly rendering their active sites in a denatured form that is permanently nonfunctional. By comparison, the benefits of using immobilized enzymes[7] are obvious and have been widely demonstrated. In addition to more convenient repeated re-utilization, immobilisation provides enhanced stability under both storage and operational conditions. This is because relatively fewer immobilized enzymes get denatured from heat, autolysis and product

Jiangsu Key Laboratory of New Power Batteries, Jiangsu Collaborative Innovation Center of Biomedical Functional Materials, Jiangsu Key Laboratory of Biofunctional Materials, College of Chemistry and Materials Science, Nanjing Normal University, Nanjing 210023, P.R. China. E-mail: sundongmei@njnu.edu.cn; Fax: +86-25-83243286; Tel: +86-25-85891651

† Electronic supplementary information (ESI) available: SEM images of the cyanogel–PB–MWCNT/Au electrode at different magnifications, digital photographs of the Sn–Fe cyanogels and the silica gel, entrapped with the same amount of GOx, after immersion in 48 mM sodium acetate buffer solution for various times, kinetic curves of GOx-bound Sn–Fe cyanogels/silica gel films in sodium acetate buffer solution, bioactivity profile of GOx entrapped in Sn–Fe cyanogels/silica gel films, the effect of temperature on the response current of the cyanogel–GOx–PB–MWCNT/Au electrode toward glucose detection. See DOI: 10.1039/c4tb00406j

‡ Both authors contributed equally to this work.

inhibition due to the limited exposure to hazardous solvents, chemical intermediates and reaction products in the liquid form. In addition, improved bioactivity and specificity could probably be obtained when a desired interaction is established between the enzymes and supports.

Much effort has been made to develop robust immobilization strategies[8–10] for the optimum performance of enzymatic biosensors. It was demonstrated that the expressed bioactivity and apparent kinetics of immobilized enzymes, which is the key point for successful design of an efficient biosensing interface, were highly dependent on factors such as the nature of the selected support and the impact of the applied immobilization technique. In accordance with the individual structure of each associated enzyme, a variety of support materials, such as inorganic and organic hydrogels[11] (polyvinyl pyridine, polyallylamine, silica gels), polysaccharide-based composites[12] (alginate, chitosan, agarose), carbon nanomaterials[13] (graphene, CNTs, fullerenes), semiconducting metal oxide (ZnO, TiO_2, CuO and Fe_3O_4) nanoparticles,[14,15] or nanostructured material-incorporated nanocomposites, combined with an appropriate immobilization method,[16–19] including sol–gel entrapment, cross-linking over a coupling agent like glutaraldehyde, electrostatic assembly, physical adsorption through hydrogen bonding, π–π stacking and electrostatic or hydrophobic interactions, and covalent attachment, respectively, were extensively investigated in the literature for elaboration of a sensitive biosensor with good selectivity and long-term stability. Among these, porous hydrogel encapsulation, especially when additionally coupled with multipoint covalent or noncovalent attachment *via* a pre- or co-entrapped nanostructured material to further avoid elution of the immobilized enzyme, has shown attractive applications in biosensors and biofuel cells, due to the advantages of cost effectiveness, easy operation, rapid detection with high reproducibility, enhanced stability, high versatility and the widespread availability of relatively simple equipment for analysis. Previous work from Betancor[20] offered a reasonably accessible method effective in reducing large leakage of entrapped enzymes from the sol–gel matrix of silica. The enzymes were pre-linked on glutaraldehyde-activated porous Sepabeads. This dramatically minimized the potential risks of direct exposure to harsh trapping conditions and negative interactions with the sol–gel components, resulting in improved enzyme bioactivity and stability. The retained final activity through pre-immobilization treatment was 92% of the initial activity, and it was considerably higher than that of 28% for the enzyme directly trapped in the sol–gel matrix. However, the selected inorganic hydrogel of silica was prepared from hydrolyzation of the organic precursor tetramethyl orthosilicate (TMOS) at an acidic pH level, where the hazardous experimental conditions and relatively high swollen structure were not suitable to maintain acceptable bioactivity and stability of the grabbed enzyme, and the incorporated porous material of the Sepabeads with an average particle size of 20 μm was too big to electrically connect with an electrode for construction of high-performance biosensors.

Cyanogels,[21,22] three-dimensional porous inorganic hydrogels, were made by simply mixing a chlorometalate and a cyanometalate in aqueous solution. The process was initiated through a ligand exchange reaction to form small cyanosol particles, in which two *trans* chloride ligands on the chlorometalate were substituted by the nitrogen ends of cyanide ligands on the cyanometalate complex, followed by a true sol–gel transition *via* strong inter-particle interactions. At the end, the resulting cyanide-bridged coordination polymer with transition-metal centers in positive oxidation states was achieved. Compared to conventional oxide-based inorganic hydrogels such as silica, obtained through polymerization of oxo species, the advantage of cyanogels for enzyme immobilization are obvious. First, they are quite simple to fabricate under mild experimental conditions with less harm to the encapsulated enzyme. Second, the structures are rigid and stable in nature without any observable change in volume, even when immersed in water for a long time. Third, they exhibit high affinity with water, typically containing >95% water by weight. When combined with the feature of controllable pore size of the three-dimensional network in a quite small range from 40 to 5 nm in radius,[23] they offer opportunities as a biocompatible matrix with a benign microenvironment for enzyme immobilization and a desirable degree of mobility both for the substrate and subsequent reaction product.

In this work, we demonstrate a novel and attractive strategy for facile enzyme immobilization, in which three-dimensional porous cyanide-bridged Sn–Fe hydrogels with desirable microenvironments for the entrapped enzyme were applied for the first time to incorporate the key bioelectrocatalytic elements of enzymes to construct a sensing and stable interface for an amperometric biosensor. It was observed that Sn–Fe cyanogels exhibited higher electrochemical inertness over wider working potential windows than other transition metal-centered cyanogels such as the Pd–Fe analogue.[24] Taking advantage of the extraordinarily high electrical conductivity, the large surface-to-volume ratio and the flexible fiber-shaped rough profile of multi-walled carbon nanotubes (MWCNTs), the prepared Sn–Fe cyanogel-entrapped enzyme-based sensing interface was successfully connected to the surface of a selected electrode support, giving sufficient accessibility to electrons to shuttle between the immobilized enzyme and the electrode. By modifying with a functional layer of Prussian blue (PB), which demonstrates high activity and selectivity toward the reduction of hydrogen peroxide, as a redox mediator through pre-electrodeposition, when glucose oxidase (GOx) was selected as a model enzyme, the resulting glucose biosensor exhibited a low detection limit of 0.1 μM (S/N 3) with improved stability. The results suggest that the Sn–Fe cyanogels with good biocompatibility and sufficient interfacial adhesion hold promise as an attractive support material and the reported protocol is amenable to a variety of enzymes for construction of reliable and durable amperometric biosensors through using an alternative functional layer instead of PB.

Experimental

Reagents

Glucose oxidase (GOx, from *Aspergillus niger*), multiwalled carbon nanotubes (MWCNTs) (>95% purity) and glucose were

purchased from Sigma Co., Ltd., Chengdu Organic Chemicals Co., Ltd., Chinese Academy of Sciences and Sinopharm Chemical Reagent Co., Ltd. (Shanghai, China), respectively, and used without further purification. Peroxidase (POD, from horseradish) and *o*-dianisidine dihydrochloride were obtained from Sigma-Aldrich and also used as purchased. All other chemicals were commercially available and of analytical grade. Distilled water was used throughout and all solutions were made using distilled water as solvent unless otherwise mentioned. The stock glucose solution (2.0 M) was allowed to mutarotate at room temperature for 24 h before use. Solutions of hydrogen peroxide (H_2O_2) were freshly diluted from the 30% solution and their concentrations were determined using a standard solution of $KMnO_4$. The supporting electrolyte used in this work was phosphate buffer (10 mM, pH 5.0) containing KCl (0.3 M) unless stated. The solution pH was adjusted by the addition of dilute KOH or HCl solution.

Electrodeposition of PB on the surface of the MWCNT-modified gold electrode

A planar gold disk electrode (CHI, 2 mm in diameter) was used as the base electrode for the modified glucose biosensor. An Au electrode was polished with alumina powder (0.05 μm) to a mirror finish and rinsed thoroughly with water after polishing, then successively washed with water and ethanol in an ultrasonic bath, then dried in air. Prior to modification, the Au electrode was pretreated by oxidation/reduction cycling in H_2SO_4 solution (0.5 M).

Preparation of the PB–MWCNT-modified electrode was carried out as reported previously.[25] Firstly, MWCNTs (4.0 μL, 1 mg mL^{-1}) were dropped on the surface of the pretreated Au electrode using a microsyringe, then dried at 40 °C. Secondly, the potential of the MWCNT-modified electrode was poised at 0.4 V in a solution containing $K_3Fe(CN)_6$ (2.0 mM), $FeCl_3$ (2.0 mM), KCl (0.1 M) and HCl (0.1 M) for 20 s, resulting in an electrodeposited film of PB. Finally, the resulting electrode was carefully washed with water and transferred into a KCl (0.1 M) and HCl (0.1 M) solution to be cycled in the potential range from −0.05 to 0.35 V at a scan rate of 50 mV s^{-1} for 25 cycles, respectively. After washing in water, it was dried in air to be used.

Fabrication of the multilayer composite electrode of cyanogel–GOx–PB–MWCNT/Au

The construction of a cyanogel–GOx–PB–MWCNT/Au electrode was accomplished on the basis of the prepared PB–MWCNT-modified Au electrode mentioned above through the following two steps. First, $SnCl_4$ (3 μL, 0.2 M) was placed on the surface of the resulting PB–MWCNT/Au electrode. Then $K_4Fe(CN)_6$ (1 μL, 0.2 M, containing 20 mg mL^{-1} GOx) was immediately cast onto the electrode as well, and allowed to dry at ambient temperature. The fabricated electrode was denoted as the cyanogel–GOx–PB–MWCNT/Au electrode. A control electrode (cyanogel–PB–MWCNT/Au) was fabricated similarly except that $K_4Fe(CN)_6$ (0.2 M) solution without added GOx enzyme was used instead. When not being used, the electrodes were stored in the refrigerator at 4 °C.

Preparation of silica gels

For comparison, silica gel, one of the most popular supporting materials for enzyme immobilization, was used as the control sol–gel matrix. The silica gel was prepared by the method reported previously[26,27] with minor modification. In brief, firstly, a mixture of 4.26 mL tetraethoxysilane (TEOS), 4.43 mL EtOH, and 1.44 mL HCl solution at 0.5 M, was sonicated for 1 h to ensure the TEOS hydrolysed completely, resulting in a clear and homogeneous solution. Then, 0.125 mL of the above mixture was taken out, followed by dropwise addition of 0.025 mL hexamethylenetetramine ($(CH_2)_6N_4$) solution at 2.5 M under sonication. After that, the obtained mixture proceeded in another 10 min sonication to accelerate the polycondensation reaction. Finally, the resulting transparent silica sol was placed in a drying oven at a temperature of 45 °C for 1 h. The silica gel–GOx complex was fabricated similarly except that the hexamethylenetetramine solution was replaced with the same solution but containing a given amount of GOx, which was kept at a concentration equal to that in the Sn–Fe cyanogels as mentioned above.

Enzymatic assay of immobilized GOx

The GOx activity entrapped in the Sn–Fe cyanogels or the silica control hydrogels were determined spectrophotometrically, based on a well-validated standard protocol from Sigma-Aldrich (http://www.sigmaaldrich.com/technical-documents/protocols/biology/enzymatic-assay-of-glucose-oxidase.html),[28] by monitoring the absorbance of oxidized *o*-dianisidine at 500 nm at different reaction times. The standard assay was carried out in 48 mM sodium acetate buffer solution at pH 5.1, containing 0.16 mM *o*-dianisidine, 1.61% (w/v) glucose, and 1.94 units per mL POD. The hydrogel matrix–enzyme composite, which was sealed in a dialysis tube with a specific Molecular Weight Cut Off (MWCO) of 8000 Da, was added to this solution at the bottom of the cuvette. Vigorous stirring was employed during the detection.

Apparatus and electrochemical measurements

Scanning electron microscopy (SEM) was performed on a JEOL JSM-7600F scanning electron microscope. Ultraviolet-visible (UV-vis) spectra were recorded on a Hitachi UV3600 spectrophotometer.

Electrochemical measurements were performed in a conventional three-electrode electrochemical cell using a CHI 660C electrochemical analyzer. A Pt plate auxiliary electrode and a saturated calomel reference electrode (SCE) were used. All potentials were measured and reported *versus* the SCE. All the electrochemical measurements were carried out at 25 ± 1 °C.

Results and discussion

Fabrication and characterization of the multilayer cyanogel–GOx–PB–MWCNT/Au nanocomposite electrode

Three-dimensional cyanide-bridged Sn–Fe hydrogels were selected, in particular, as a novel matrix for enzyme immobilization, because of their desirable microenvironment, ease to be

made and extra high stability. When a freshly-made $K_4Fe(CN)_6$ solution was added to an amount of $SnCl_4$ solution, the instant formation of a hydrated three-dimensional (3D) porous Sn–Fe network was observed, as shown in Fig. 1a, in which the fabricated cyanogels stayed in the vial even while flipped upside down. No obvious change was found at room temperature over three months, as shown in Fig. 1b, indicating that it is extremely stable on its own, without excessive costs.

Further studies indicated that the morphological stability of the rigid cyanogel matrix was highly dependent on the pH value of the selected incubation solution. As shown in Fig. 2, under a solution with pH greater than 8.0, it became unstable and was gradually destroyed and finally collapsed, though structural integrity was maintained in acidic solutions, especially when the pH is less than 6.0. Accordingly, buffer solution at pH 5.0, which was also the optimum pH of the model enzyme, was chosen as supporting electrolyte in the following research experiments.

The greatest difficulty to construct a sensitive and stable interface for an amperometric biosensor based on the stable Sn–Fe hydrogels mentioned above, was to find a way to effectively fix the enzyme-entrapped hydrogel to a conductive electrode support, giving sufficient accessibility for electrons to shuttle between the immobilized enzyme and the electrode. Our facile three-step strategy for a cyanogel–GOx–PB–MWCNT/Au composite electrode was first reported and demonstrated as shown schematically in Scheme 1, in which GOx was chosen as a model enzyme. First, the pretreated Au electrode was modified with MWCNTs to ensure good electronic contact between the electrode and the 3D sensing interface built in the third step. Second, PB was electrodeposited on the surface of the adsorbed MWCNTs to create a functional layer for quantitative measurement of the electroactive species of H_2O_2 produced from the enzymatic breakdown of glucose *via* the immobilized enzyme GOx. Third, an *in situ*-produced 3D network of Sn–Fe cyanogels containing pre-immobilized GOx enzyme was incorporated into the constructed rough layer of PB–MWCNT complexes, providing a desirable microenvironment for the entrapped enzyme. The large surface-to-volume ratio and the flexible fiber-shaped rough profile of the MWCNTs, combined with the electrodeposited PB, which share similar structure and several material properties with finally capped Sn–Fe cyanogels, made it possible to create a successful connection between the enzyme-entrapped hydrogel and conductive electrode support.

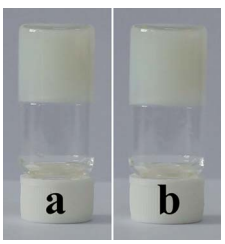

Fig. 1 Digital photographs of the cyanogels. (A) 2 min, (B) three months.

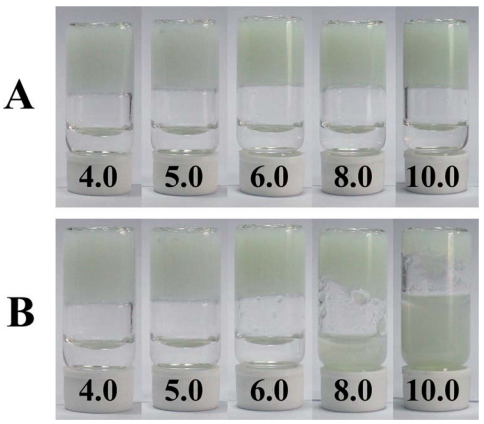

Fig. 2 Digital photographs of the cyanogels in solutions at various pH levels (A) before and (B) after 3 weeks under ambient temperature.

SEM was used to characterize the successful fabrication step-by-step and to investigate the three-dimensional hierarchical morphological structure of the as-prepared MWCNT-grafted Sn–Fe cyanogels functionalized with electrodeposited PB on the surface of a Au electrode. The image of the first step after the MWCNTs were modified on the surface of the Au electrode shown in Fig. 3A indicated that the MWCNTs were dispersed evenly on the entire surface and almost uniformly distributed without aggregation, with an average size that was found to be 25 ± 8 nm in diameter. The complementary technique of atomic-resolution elemental mapping by SEM with energy dispersive X-ray spectrometry (EDS) was applied for further qualitative analysis. As illustrated in the inset of Fig. 3A taken within the area bordered by a dashed yellow line, abundant carbon was detected, providing follow-up confirmation of the existence of MWCNTs. Subsequently, the element Fe was detected, distributed evenly across a similar area, as shown in the inset of Fig. 3B, when PB was sequentially electrodeposited onto the surface of the MWCNT/Au. In addition, there was no obvious surface morphology change (Fig. 3B) following the second step, except for a small increase in the diameter of the MWCNTs, indicating that electrodeposition happened on the surface of the MWCNTs, leaving enough rough space for the incorporation of the next key material of the cyanogel matrix.

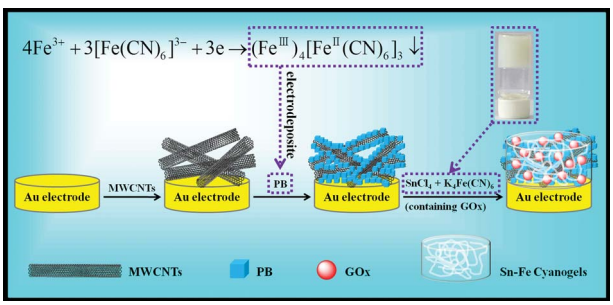

Scheme 1 Schematic illustration of the prepared MWCNT-grafted Sn–Fe cyanogel entrapped GOx modified electrode with a functional layer of PB.

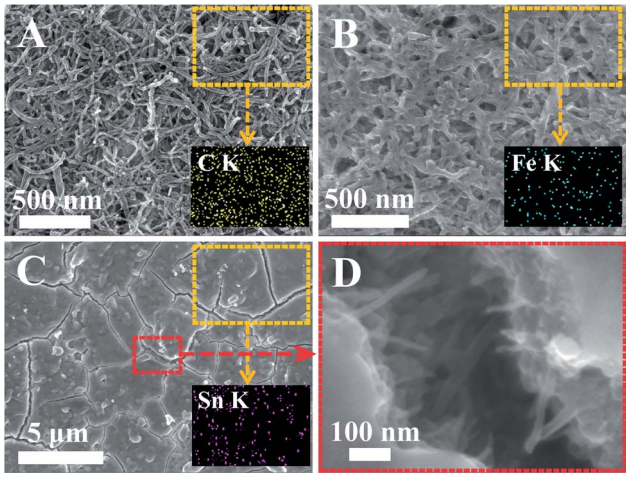

Fig. 3 SEM images of (A) the MWCNT/Au, (B) the PB–MWCNT/Au and (C) the cyanogel–GOx–PB–MWCNT/Au electrodes ((D) shows a magnified view of the crack of the cyanogel–GOx–PB–MWCNT/Au).

Images of the final step, as shown in Fig. 3C, indicated that the presence of element Sn in a continuum distribution was clearly observed (inset, Fig. 3C) and the surface became less rough and smoother, demonstrating that cyanide-bridged Sn–Fe hydrogels were effectively grafted to the MWCNT surfaces. The inner structure of the freshly-made biosensing interface was revealed in the magnified view (Fig. 3D) at the vicinity of the crack location bordered by a dashed red line in Fig. 3C, in which there were individual MWCNTs sticking out from the inside. In addition, the control electrode of cyanogel–PB–MWCNT/Au has a very similar outward appearance (shape, structure, pattern) to that of cyanogel–GOx–PB–MWCNT/Au (Fig. S1 in ESI†), indicating that the incorporation of GOx made little change to the formation of the cyanogels and the reproducibility of the proposed electrode is quite good. These results exhibit the success of our facile three-step strategy for fabrication of a cyanogel–GOx–PB–MWCNT/Au composite electrode, with a multilayer configuration that was well-organized as proposed, consistent with the following experimental observations.

The UV-vis absorption spectra of pristine GOx, cyanogel-entrapped GOx, and a pure Sn–Fe cyanogel matrix were similarly measured over the range of 200 to 600 nm in PBS solution at a pH of 5.0, to examine the effectiveness of the proposed enzyme immobilization strategy mentioned above. As shown in Fig. 4, Sn–Fe cyanogels (Fig. 4b) exhibit featureless adsorption in the wavelength range of interest, whereas cyanogel–GOx (Fig. 4c) displayed obvious absorption around 276.8 nm and two more weak peaks around 381.6 nm and 454.1 nm, respectively, all of which were attributed to characteristic bands of the enzyme GOx,[29] confirming the encapsulation of GOx inside the 3D porous Sn–Fe cyanogel backbone. The relatively low intensities of both absorption bands around 381.6 nm and 454.1 nm showed that the entrapped GOx was not at a very high concentration in the collected sample. Except for lower absorption intensity corresponding to lower concentration, and a relatively broader peak width at *ca.* 276.8 nm, due to the possible weak interaction between the immobilized enzyme and the matrix, the features of

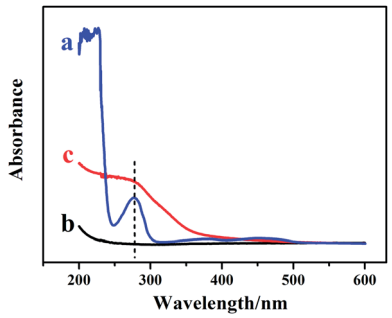

Fig. 4 UV-vis spectra of (a) native GOx in PBS buffer solution (pH 5.0), (b) a cyanogel sample and (c) a GOx–cyanogel sample.

GOx in the GOx–cyanogel composite film were almost the same as those of pristine GOx (Fig. 4a), indicating no significant influence on the spectral characteristics of GOx after it was embedded. This demonstrated the good fidelity of the active site of the entrapped GOx and the effective immobilization of GOx, with good retention of biological activity as demonstrated by the following electrochemical results as well.

Electrochemical properties of the MWCNT-grafted Sn–Fe cyanogel entrapped GOx modified electrode with a functional layer of PB

GOx is an FAD-dependent enzyme that catalyzes the oxidation of β-D-glucose by molecular oxygen, and is most commonly used for the construction of glucose biosensors. The electrochemical activity of GOx incorporated in the cyanogel–PB–MWCNT nanocomposite was investigated. Fig. 5 presents the cyclic voltammograms of a cyanogel–GOx–PB–MWCNT-modified Au electrode (curve b) relative to the cyanogel–PB–MWCNT/Au control electrode (curve a). A typical CV peak response centered around 0.174 V, similar to that as reported in the literature,[30–32] toward the redox couple of PB and Prussian white, was observed for the cyanogel–PB–MWCNT-modified Au electrode control in 10 mM PBS containing 0.3 M KCl, pH 5.0, at 50 mV s^{-1} within

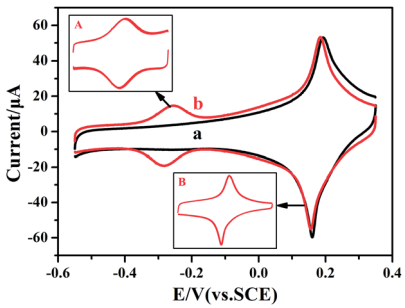

Fig. 5 Cyclic voltammograms of (a) the cyanogel–PB–MWCNT/Au and (b) cyanogel–GOx–PB–MWCNT/Au electrodes in a 10 mM PBS solution (pH 5.0) containing 0.3 M KCl at a scan rate of 50 mV s^{-1}. Inset: (A) cyclic voltammograms of the cyanogel–GOx–PB–MWCNT/Au electrode after 100 continuous cycles at −0.45 V ∼ −0.1 V and (B) cyclic voltammograms of the cyanogel–GOx–PB–MWCNT/Au electrode after 200 continuous cycles at −0.05 V to 0.4 V.

the potential range of −0.55 to +0.35 V, confirming the formation of the hybrid composite of PB–MWCNTs in the second round of experiments. The calculated separation of peak potentials, ΔE_p, for the anodic and cathodic peaks equal to 31 mV was quite low, indicating the facile electron transfer between the electrodeposited PB and the Au electrode, which is one of the key points for the construction of an efficient biosensing interface based on Sn–Fe cyanogels, as the PB was acting as a functional layer to facilitate electron transfer between the immobilized enzyme and the supporting Au electrode. Fig. 6 shows the cyclic voltammograms of the PB within cyanogel–GOx–PB–MWCNT/Au in 10 mM PBS (pH 5.0) containing 0.3 M KCl at various scan rates (v). The E_{pa} shifts positively and E_{pc} shifts negatively with increasing scan rate ranging from 10 up to 100 mV s^{-1}, yielding a formal potential (defined as the average of the anodic and cathodic peak potentials), $E^{0\prime} = -(0.174 \pm 0.004)$ V, which remained practically invariant across all scan rates, as shown in Fig. 6A. In addition, the anodic peak current (i_{pa}) and cathodic peak current (i_{pc}) were found to vary linearly as a function of the scan rate (Fig. 6B), suggesting that the reaction is a surface-controlled process, commonly observed in systems employing immobilized electroactive species.

In contrast, the cyanogel–PB–MWCNT-modified Au electrode with immobilized GOx showed two pairs of distinct and nearly symmetric redox peaks, indicating the presence of another faradaic species except for PB. The first pair of quasi-reversible redox peaks, characteristic of electroactive species of PB as demonstrated above, exhibited no clear variations either in peak potential or peak current when compared with that of the control electrode, as did the capacitive current within the whole potential range of the positive going scan, indicating that a high quality reproducible protocol for construction of enzyme-based biosensing interfaces was established. The newly-appeared anodic peak potential (E_{pa}) and cathodic peak potential (E_{pc}) were located at −0.258 and −0.281 V, respectively, against the reference. Obviously, the presence of the second pair of redox peaks was attributed to an electrochemical reaction of the physically entrapped GOx between GOx–FAD and GOx–$FADH_2$, *via* the promotion of the Sn–Fe cyanogels, which provide a three-dimensional stage for enzyme immobilization. The ΔE_p for the anodic and cathodic peaks of GOx was calculated to be 23 mV, which is smaller compared to that found in the literature.[33] This suggests that the preferred orientation of the immobilized GOx on the surface of the Au electrode was obtained in the presence of Sn–Fe cyanogels, which induces very effective electron transfer from the FAD of GOx to the Au electrode. Since the i_{pc} was almost equal to the i_{pa}, the immobilized GOx appears to undergo a quasi-reversible electrochemical reaction. Its formal potential, $E^{0\prime}$, is −0.270 V at a scan rate of 50 mV s^{-1}, which is more positive than the result of that reported previously.[34,35] This suggests that most of the biomolecules preserved their original structure even after being entrapped in the Sn–Fe cyanogels, which is in good agreement with the result from the UV-vis spectroscopic characterization. The positive shift of the peak potentials is presumably attributed to the presence of the MWCNT-grafted Sn–Fe cyanogels, which have a positive effect on the redox reaction of the immobilized GOx.

Alternative attention was paid to a detailed investigation of the redox behaviour of the PB in the cyanogel–GOx–PB–MWCNT biosensing interface to obtain the optimized experimental conditions, assuring the proposed biosensor has maximum sensitivity for the detection of trace glucose. Fig. 7 shows the pH dependencies of the peak currents of PB in various pH media from 4.0 to 7.4 buffered by 10 mM phosphate. The cathodic peak currents decreased sharply as the medium pH, greater than 5.0, increased, whereas no apparent change was observed in more acidic solutions. This is in good agreement with the fact that PB exhibits a tendency to decompose under alkaline conditions, as reported previously.[36] Taking several factors into consideration, such as enzymatic activity, and PB and Sn–Fe cyanogel stability, which were studied as shown above, the electrolyte was then buffered at a pH of 5.0 in this work. Simultaneously, the effect of different concentrations of the KCl

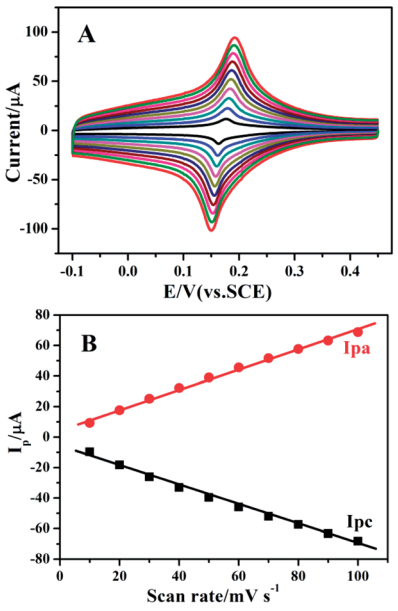

Fig. 6 (A) Cyclic voltammograms of the cyanogel–GOx–PB–MWCNT/Au electrode in a 10 mM PBS solution (pH 5.0) containing 0.3 M KCl at various scan rates. (B) Plots of the corresponding cathodic and anodic peak currents of the cyanogel–GOx–PB–MWCNT/Au electrode *vs.* scan rate.

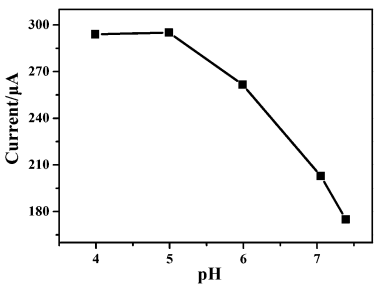

Fig. 7 Effect of pH on the reduction peak current of the PB–MWCNT/Au electrode.

supporting electrolyte, ranging from 0 to 0.4 M, on the electrochemical response of PB was examined as well, as shown in Fig. 8. An evident decrease in the value of the peak current (Fig. 8A) and an increase in peak separation (Fig. 8B) as the amount of added KCl decreased, was found, probably due to the effect of IR drop. When the final KCl concentration in the electrolyte solution was higher than 0.3 M, the ΔE_p for the redox peaks of PB almost reached the minimum value of 31 mV, displaying stable and fast electron transfer kinetics as a result of negligible electrical resistivity of the solution. Therefore, electrolyte with KCl at a concentration of 0.3 M was used in this work. These results imply that it is necessary to take into account the effect of the ionic strength of the electrolyte for this type of quantitative analysis of an electrochemical biosensor.

The stability of the prepared sensing electrode, based on GOx immobilized *via* Sn–Fe cyanogels, was examined by monitoring the CV peak current in 10 mM PBS with 0.3 M KCl using the same electrode over a period of time. After continuous CV cycling over as many as 200 cycles, shown in insets (A) and (B) of Fig. 5, neither the shape of the CV curve nor the potential and current of the redox peaks, both for PB and GOx, changed obviously, demonstrating a high within-session stability of the electrode, which could be attributed to the structural integrity during repeated running cycles as a result of negligible dissolution or aggregation of the active species involved. Similar results were observed when CV cycling was carried out at different running intervals, as shown in Fig. 9A, except for a small change in the peak current of one of the electroactive PB species, thus further confirming the desirable stability of the constructed nanocomposite biosensing interface.

In parallel, the stability of the bioelectrode was examined periodically through the possible leakage of immobilized enzymes recorded by UV-visible experiments. As shown in Fig. 9B, negligible leakage of the GOx enzyme immobilized in the matrix of the Sn–Fe cyanogels, was observed, which is in good agreement with the results obtained from the electrochemical experiments presented above. Moreover, the corresponding enzymatic assay (Fig. S3 in ESI†) shows that the immobilized enzyme in the Sn–Fe cyanogels lost only about 4% of its initial activity in the first 5 h, while more than 87% of the initial activity was kept even after 7 days of immersion in 48 mM sodium acetate buffer solution (pH 5.1) at 4 °C, the same buffer as used in the enzymatic assay. These results also demonstrate the efficient and stable holding of the immobilized enzyme in an active state in the matrix of the Sn–Fe cyanogels. However, by contrast, when the control sol–gel matrix of silica, one of the most popular supporting materials for enzyme immobilization, was used, large leakage of the entrapped enzymes was observed, since the as-prepared silica gel–GOx composite was turning from yellow almost back to transparent after 7 days of immersion, though almost no color change can be identified for the Sn–Fe cyanogel–GOx composite under the same experimental conditions (Fig. S2 in ESI†). In addition, the initial activity of the immobilized enzyme in silica gel was only about 33% of that in Sn–Fe cyanogels (curve d and column d, Fig. S3 in ESI†), which can be attributed to the direct exposure to harsh trapping conditions and negative interactions with the sol–gel components as explained above. Furthermore, there was almost no detected activity after 7 days of immersion (curve f and column f, Fig. S3 in ESI†), probably caused by the elution of the immobilized enzyme, which is in good agreement with what

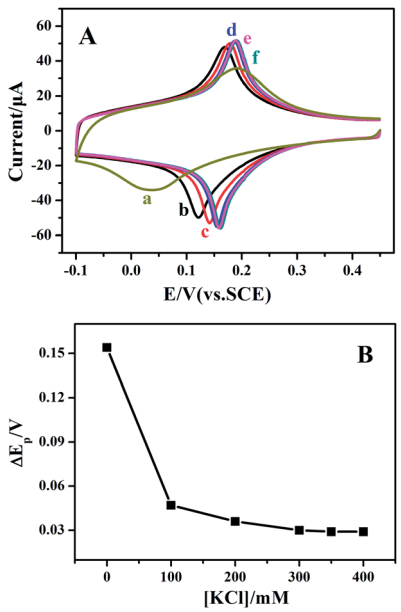

Fig. 8 (A) Cyclic voltammograms of the cyanogel–GOx–PB–MWCNT/Au electrode in 10 mM PBS solution (pH 5.0) containing (a) 0, (b) 0.1, (c) 0.2, (d) 0.3, (e) 0.35 and (f) 0.4 M KCl at a scan rate of 50 mV s^{-1}. (B) The effect of KCl concentration on the redox peak potential difference.

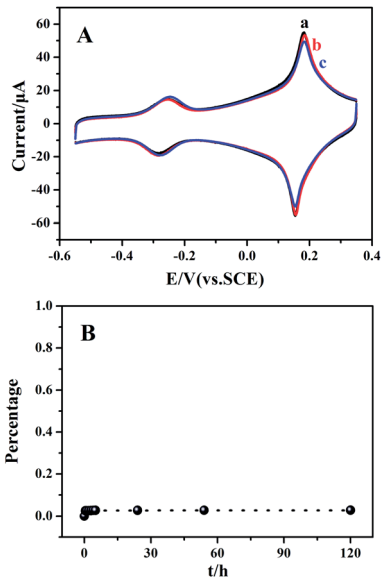

Fig. 9 (A) Cyclic voltammograms of the cyanogel–GOx–PB–MWCNT/Au electrode in 10 mM PBS solution (pH 5.0) containing 0.3 M KCl. (a) 1 h, (b) 24 h, (c) 120 h. (B) Leakage percentage of GOx entrapped in Sn–Fe cyanogels exposed to 10 mM PBS solution determined at different soaking intervals by UV-visible spectrophotometry.

was observed regarding the color change of the silica gel–GOx composite. On the other hand, though the stability of the immobilized enzyme is much higher than that of the free enzyme un-immobilized in solution, for the electrochemical activity, the free enzyme is usually much better than that of the immobilized one.[37,38]

Analytical performance of the prepared cyanogel–GOx–PB–MWCNT/Au for efficient biosensing of glucose

PB has proved to be a powerful electrocatalyst for the analytical determination of H_2O_2 with potential application as an efficient amperometric transducer for the development of oxidase-enzyme-based biosensors.[39] As a matter of fact, PB-promoted biosensing operates in a cathodic manner (eqn (4)), therefore, the problems of non-specific oxidation of interfering species usually present in biological samples, such as ascorbate, urate, and paracetamol, can be avoided by using PB-integrated biosensors, resulting in high selectivity to the specific substrate of the immobilized enzyme as expected.

In the absence of immobilized GOx, the electrocatalytic behavior of the electrodeposited PB incorporated with the cyanogel–MWCNT-modified Au electrode was investigated, as shown in Fig. 10. Following the addition of 10.19 mM H_2O_2, the shape of the cyclic voltammograms of the cyanogel–PB–MWCNT/Au electrode changed significantly, and was characterized by a large cathodic peak starting at *ca.* 0.304 V (Fig. 10, curves a to g), attributed to the electrocatalytical reduction of H_2O_2. An increase in the concentration of H_2O_2 was accompanied by an increase in the reduction currents and a decrease in the oxidation currents. The electrode linearly responded to H_2O_2 with a good linear range obtained from 0.59 up to 10.19 mM ($R = 0.996$).

In the presence of immobilized GOx, combined with a highly sensitive method of differential pulse voltammetry (DPV), under optimized experimental conditions, the resulting biosensor based on MWCNT-grafted Sn–Fe cyanogels and enhanced with a functional layer of PB exhibited great performance for detection of glucose. Fig. 11A displays the differential pulse voltammograms of the cyanogel–GOx–PB–MWCNT/Au electrode, in 10 mM PBS with 0.3 M KCl containing various concentrations of successively dropped glucose, at 20 mV s^{-1}, within the PB-active potential range of −0.05 to +0.40 V. Upon addition of glucose, the current response increased (Fig. 11A), contributing to an immediate introduction of H_2O_2, which was *in situ* produced from the GOx/glucose reaction, and subsequently reduced by the efficient and sensitive PB catalyst incorporated inside the transducing surface of the proposed biosensor. The reactions involved in this process are portrayed as follows:

$$Fe_4^{III}[Fe^{II}(CN)_6]_3 \text{ (PB in oxidized form)} + 4e^- + 4K^+ \rightarrow K_4Fe_4^{II}[Fe^{II}(CN)_6]_3 \text{ (Prussian white)} \quad (1)$$

$$\beta\text{-D-glucose} + O_2 + H_2O \xrightarrow{GOx} \text{D-gluconic acid} + H_2O_2 \quad (2)$$

$$K_4Fe_4^{II}[Fe^{II}(CN)_6]_3 + 2H_2O_2 \rightarrow Fe_4^{III}[Fe^{II}(CN)_6]_3 + 4K^+ + 4OH^- \quad (3)$$

As a result, a net electrochemical reaction of cathodic peroxide reduction proceeds:[40]

$$H_2O_2 + 2e^- \xrightarrow{PB} 2OH^- \quad (4)$$

The reduction current of the cyanogel–GOx–PB–MWCNT/Au electrode has a positive correlation with the concentration of glucose, which is the general feature of electrocatalytic

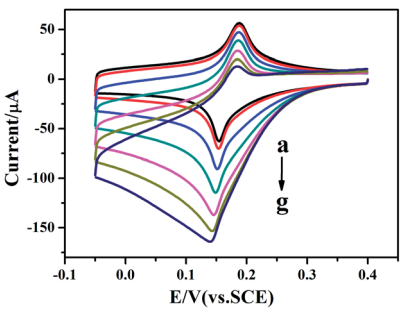

Fig. 10 Cyclic voltammograms of the cyanogel–PB–MWCNT/Au electrode in 10 mM PBS (pH 5.0) with 0.3 M KCl containing (a) 0, (b) 0.59, (c) 2.19, (d) 4.19, (e) 6.19 (f) 8.19 and (g) 10.19 mM H_2O_2 at a scan rate of 50 mV s^{-1}.

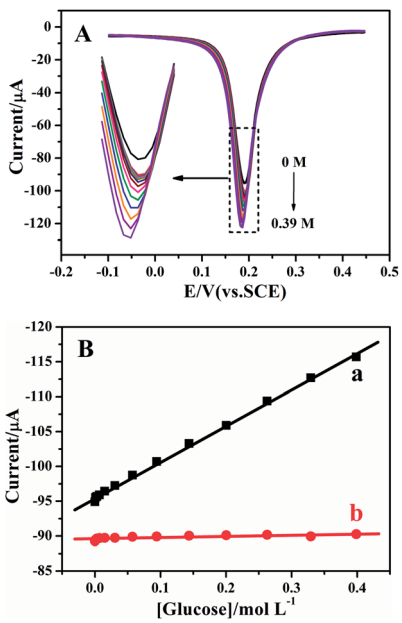

Fig. 11 (A) A series of differential pulse voltammograms of the cyanogel–GOx–PB–MWCNT/Au electrode in a 10 mM PBS solution (pH 5.0) with 0.3 M KCl containing 0, 1.00×10^{-6}, 9.98×10^{-4}, 2.99×10^{-3}, 6.96×10^{-3}, 1.48×10^{-2}, 3.05×10^{-2}, 9.42×10^{-2}, 1.43×10^{-1}, 2.00×10^{-1}, 2.62×10^{-1}, 3.29×10^{-1} and 3.99×10^{-1} M glucose (from top to bottom). Pulse amplitude, 50 mV; sample width, 20 ms; pulse width, 50 ms; scan rate, 20 mV s^{-1}; sensitivity, 100 μA V^{-1}. (B) Plot of the reduction peak current *versus* glucose concentration for (a) the cyanogel–GOx–PB–MWCNT/Au electrode and (b) the cyanogel–PB–MWCNT/Au control electrode.

reactions for the application of substrate sensing, whereas no response current change for the cyanogel–PB–MWCNT/Au control electrode was observed with the addition of glucose at the same concentration range of interest (curve b, Fig. 11B). As shown in curve a, Fig. 11B, the obtained linear dependence of the response current on glucose concentration was from 1.00×10^{-6} M up to 3.99×10^{-1} M ($R = 0.9992$). It is noted that the dynamic linear range in our scheme is quite desirable, especially for the determination of glucose in samples from physiological systems, since, as an example, plasma glucose is normally found at a concentration in the range of 3.7–5.6 mM when tested in non-diabetics while fasting.[41] Within the linear response range, the calculated sensitivity was 1.68 μA mM^{-1} cm^{-2}. The apparent surface area of the electrode was estimated using the method reported previously.[42] The limit of detection was estimated to be as low as *ca.* 0.1 μM (at *S*/*N* 3), comparable to the values reported in the literature.[43] These results indicated that GOx retains its robust bioelectrocatalytic activity after being encapsulated into the Sn–Fe cyanogels due to the enhanced biocompatible microenvironment, and further confirmed that the immobilized GOx still retained its essential secondary structure, as proved spectrophotometrically.

More experiments were carried out to explore the temperature effect on the electrocatalytic activity of the immobilized GOx in cyanogel–PB–MWCNT/Au toward glucose detection. An increase in activity with temperature was observed (Fig. S4 in ESI†). This is an Arrhenius-type relationship commonly observed in enzymatic reaction systems.

Conclusions

A facile three-step strategy for construction of an efficient and reliable biosensing interface based on immobilized enzyme entrapped inside Sn–Fe cyanogels, with electrodeposited PB at the transducing surface as a versatile electrocatalyst, and adsorbed MWCNTs between the underlying electrode and the redox enzyme GOx as a molecular wire to enhance electron transfer, was developed. The analytical performance of the resulting cyanogel–GOx–PB–MWCNT/Au electrode, similar to those in the literature, toward the electrocatalytic oxidation of glucose, was clearly demonstrated. The experimental results reveal that the developed amperometric biosensor for glucose determination exhibits low detection limit and great analytical sensitivity with long-term stability. The Sn–Fe cyanogels with attractive properties are a promising matrix for enzyme immobilization and the proposed protocol for versatile enzyme immobilization has paved the way for the construction of sensitive and stable amperometric biosensors with a wide range of applications, such as for glucose monitoring in blood when GOx was selected as the biocatalyst.

Acknowledgements

The authors thank the financial support from NSFC (no. 21005039), the Project (no. Y207K5) supported by the Key Laboratory of Renewable Energy, Chinese Academy of Sciences and the Project Funded by the Priority Academic Program Development (PAPD) of Jiangsu Higher Education Institutions.

Notes and references

1 S. M. Lane, Z. Kuang, J. Yom, S. Arifuzzaman, J. Genzer, B. Farmer, R. Naik and R. A. Vaia, *Biomacromolecules*, 2011, **12**, 1822.
2 A. Sassolas, L. J. Blum and B. D. Leca-Bouvier, *Biotechnol. Adv.*, 2012, **30**, 489.
3 R. A. Sheldon, *Adv. Synth. Catal.*, 2007, **349**, 1289.
4 Y. H. Kim, E. Campbell, J. Yu, S. D. Minteer and S. Banta, *Angew. Chem., Int. Ed.*, 2013, **52**, 1437.
5 B. Reuillard, A. Le Goff, M. Holzinger and S. Cosnier, *J. Mater. Chem. B*, 2014, **2**, 2228.
6 C. Garcia-Galan, Á. Berenguer-Murcia, R. Fernandez-Lafuente and R. C. Rodrigues, *Adv. Synth. Catal.*, 2011, **353**, 2885.
7 Y. Chen, B. Jin, L. R. Guo, X. J. Yang, W. Chen, G. Gu, L. M. Zheng and X. H. Xia, *Chem. –Eur. J.*, 2008, **14**, 10727.
8 S. P. Cullen, I. C. Mandel and P. Gopalan, *Langmuir*, 2008, **24**, 13701.
9 N. Vasylieva, C. Maucler, A. Meiller, H. Viscogliosi, T. Lieutaud, D. Barbier and S. Marinesco, *Anal. Chem.*, 2013, **85**, 2507.
10 P. Huang, J. Mao, L. Yang, P. Yu and L. Mao, *Chem. –Eur. J.*, 2011, **17**, 11390.
11 E. I. Yashina, A. V. Borisova, E. E. Karyakina, O. I. Shchegolikhina, M. Y. Vagin, D. A. Sakharov, A. G. Tonevitsky and A. A. Karyakin, *Anal. Chem.*, 2010, **82**, 1601.
12 W. Suginta, P. Khunkaewla and A. Schulte, *Chem. Rev.*, 2013, **113**, 5458.
13 Q. Zhang, Y. Qiao, F. Hao, L. Zhang, S. Wu, Y. Li, J. Li and X. M. Song, *Chem. –Eur. J.*, 2010, **16**, 8133.
14 X. Luo and L. Zhang, *Biomacromolecules*, 2010, **11**, 2896.
15 Z. D. Gao, Y. Han, Y. Wang, J. Xu and Y. Y. Song, *Sci. Rep.*, 2013, **3**(3323), 1.
16 E. Kokufuta and E. Jinbo, *Macromolecules*, 1992, **25**, 3549.
17 O. Yehezkeli, Y. M. Yan, I. Baravik, R. Tel-Vered and I. Willner, *Chem. – Eur. J.*, 2009, **15**, 2674.
18 L. S. Wong, J. Thirlway and J. Micklefield, *J. Am. Chem. Soc.*, 2008, **130**, 12456.
19 J. M. Bolivar and B. Nidetzky, *Langmuir*, 2012, **28**, 10040.
20 L. Betancor, F. López-Gallego, A. Hdalgo, M. Fuentes, O. Podrasky, G. Kuncova, J. Guisán and R. Fernandez-Lafuente, *Biomacromolecules*, 2005, **6**, 1027.
21 M. Vondrova, C. M. Burgess and A. B. Bocarsly, *Chem. Mater.*, 2007, **19**, 2203.
22 J. Xu, X. Liu, Y. Chen, Y. Zhou, T. Lu and Y. Tang, *J. Mater. Chem.*, 2012, **22**, 23659.
23 S. L. Sharp and A. B. Bocarsly, *Chem. Mater.*, 1998, **10**, 825.
24 D. Iveković, S. Milardović and B. S. Grabarić, *Biosens. Bioelectron.*, 2004, **20**, 872.
25 T. Li, Z. Yao and L. Ding, *Sens. Actuators, B*, 2004, **101**, 155.
26 J. Jia, B. Wang, A. Wu, G. Cheng, Z. Li and S. Dong, *Anal. Chem.*, 2002, **74**, 2217.

27 H. Zhang, L. Fu, S. Wang, Q. Meng, K. Yang and J. Ni, *Mater. Lett.*, 1999, **38**, 260.
28 H. Bergmeyer, K. Gawehn and M. Grassl, *Methods Enzym. Anal.*, 1974, **1**, 457.
29 B. E. P. Swoboda and V. Massey, *J. Biol. Chem.*, 1965, **240**, 2209.
30 D. Du, M. Wang, Y. Qin and Y. Lin, *J. Mater. Chem.*, 2010, **20**, 1532.
31 J. Li, J. D. Qiu, J. J. Xu, H. Y. Chen and X. H. Xia, *Adv. Funct. Mater.*, 2007, **17**, 1574.
32 A. A. Karyakin, E. E. Karyakina and L. Gorton, *Anal. Chem.*, 2000, **72**, 1720.
33 M. V. Jose, S. Marx, H. Murata, R. R. Koepsel and A. J. Russell, *Carbon*, 2012, **50**, 4010.
34 V. Mani, B. Devadas and S. M. Chen, *Biosens. Bioelectron.*, 2013, **41**, 309.
35 P. Si, P. Chen and D. H. Kim, *J. Mater. Chem. B*, 2013, **1**, 2696.
36 N. B. Li, J. H. Park, K. Park, S. J. Kwon, H. Shin and J. Kwak, *Biosens. Bioelectron.*, 2008, **23**, 1519.
37 Y. Piao, D. J. Han and T. S. Seo, *Sens. Actuators, B*, 2014, **194**, 454.
38 W. J. Sung and Y. H. Bae, *Biosens. Bioelectron.*, 2003, **18**, 1231.
39 Z. D. Gao, Y. Y. Han, Y. C. Li, M. Yang and Y. Y. Song, *Electrochim. Acta*, 2014, **125**, 530.
40 A. A. Karyakin, E. E. Karyakina and L. Gorton, *Electrochem. Commun.*, 1999, **1**, 78.
41 S. C. Port, M. O. Goodarzi, N. G. Boyle and R. I. Jennrich, *Am. Heart J.*, 2005, **150**, 209.
42 Y. Chen, X. Yang, B. Jin, L. Guo, L. Zheng and X. H. Xia, *J. Phys. Chem. C*, 2009, **113**, 4515.
43 G. Fu, X. Yue and Z. Dai, *Biosens. Bioelectron.*, 2011, **26**, 3973.